

## MICROSTRUCTURE, STRENGTH AND FATIGUE OF AN ULTRAFINE-GRAINED Al-Cu-Mg ALLOY

E. Khafizova<sup>1\*</sup>, R. Islamgaliev<sup>1,3</sup>, G. Klevtsov<sup>2</sup>, E. Merson<sup>2</sup>

<sup>1</sup>Ufa State Aviation Technical University, 12 K. Marx, Ufa, 450000, Russian Federation

<sup>2</sup>Togliatti State University, 14 Belorusskaya, Togliatti, 445667, Russian Federation

<sup>3</sup>Kazan Federal University, Kremlevskaja str. 18, Kazan, Russian Federation

\*e-mail: ela.90@mail.ru

**Abstract.** The impact of equal-channel angular pressing (ECAP) on the microstructure of an Al-Cu-Mg alloy has been investigated using transmission electron microscopy and electron backscatter diffraction. A combination of an ultrafine-grained and bimodal structure was observed in the alloy as a result of ECAP processing. The ECAP-processed samples after tensile tests and cyclic loads have demonstrated an enhanced ultimate tensile strength and fatigue endurance limit in comparison with the properties of the samples subjected to the standard T6 treatment.

### 1. Introduction

It is known that Al alloys of the Al-Cu-Mg system are widely used in industry as structural materials. At the same time, there remains a topical task to enhance their strength and fatigue in order to expand their application areas in the aircraft industry and increase the lifetime of parts.

One of the ways to solve this task is to produce an ultrafine-grained (UFG) structure by means of severe plastic deformation (SPD) processing [1-7].

At present, it is known that grain refinement is accompanied by a significant enhancement of strength and lowering of ductility in various metals and alloys [8-15]. Alongside with that, the structure and mechanical properties of UFG Al alloys depend on the regimes of severe plastic deformation and the material's chemical composition, which determine the contribution of solid-solution strengthening and precipitation hardening. In addition, an enhanced grain boundary diffusion in UFG materials can lead to a decrease in the temperature and time of aging required for the precipitation of dispersed particles [8, 16-19]. In its turn, the phase composition, volume fraction and a size of precipitates may have a significant effect on the strength and fatigue of UFG Al alloys. Therefore, defining the UFG structure parameters which lead to an enhancement of the strength and fatigue properties in Al alloys is an important task.

As shown in [20-25] the grain refinement in Al alloys does not always lead to increase of fatigue. At the present time, two approaches for increasing the fatigue of UFG materials are proposed. The first approach is based on additional annealing of SPD samples, which results in a reduction of the dislocation density and internal stresses. The second approach is the creation of a bimodal structure where micrometer-sized grains are responsible for the material's ductility, and nano-sized grains provide the enhanced strength [7]. The second

approach has been implemented only for Cu samples, and it has not been sufficiently studied by now [7, 24]. As a result of the above, the structural features determining the strength and fatigue properties of UFG Al alloys still remains an object of study.

The purpose of this study is to establish the relationship between the UFG structure and the strength and fatigue of an Al-Cu-Mg alloy processed by ECAP.

## 2. Experimental

As the material under study, an Al-Cu-Mg alloy was selected. The chemical composition of the alloy according to the optical emission analysis is presented in Table 1.

Table 1. Chemical composition of the Al-Cu-Mg alloy, wt.%.

Al	Cu	Mg	Ni	Si	Fe	Mn	Cr	Zn	Ti
Balance	2.482	1.474	1.060	0.211	1.159	0.057	0.082	0.033	0.056

The ultrafine-grained (UFG) samples processed by equal-channel angular pressing (ECAP) were investigated in comparison with the coarse-grained (CG) samples after the standard T6 treatment (quenching + aging). Standard treatment (T6) included: heating to a temperature of 530 °C, holding at this temperature for 1 hour, water quenching, aging at a temperature of 190 °C for 7 hours, air cooling. SPD processing by ECAP was conducted at temperatures of 160 °C, with 2 passes (the channels intersection angle was  $\phi=90^\circ$ ) via route B<sub>c</sub>.

The heat release was recorded using a Netzsch 409 PC Luxx synchronous thermal analyzer, at a constant heating rate of 10 K/min, using platinum crucibles. All the scanning was performed in a temperature range of 25 °C to 350 °C. The samples for the calorimetric studies were cut out to have a diameter of 4 mm and a thickness of 1 mm.

The UFG structure was investigated using a JEM-2100 transmission electron microscope (TEM) with an INCAx-sight attachment which allowed conducting an elemental energy-dispersive analysis with a minimum area of 30 nm. The samples for the TEM studies were prepared by twin jet electro-polishing on a Tenupol-5 facility in an electrolyte of the following composition: 75 % methanol and 25 % nitric acid. Misorientations were investigated using a ZEISS SIGMA scanning electron microscope (SEM) with an EDAX attachment for analyzing the Kikuchi lines in the diffraction patterns. The error in measuring the grain misorientations was 0.1 deg.

The Vickers microhardness was measured on a Buehler Omnimet tester across a sample diameter with a step of 1 mm, loading of 0.1 kg for 10 s.

To test the mechanical properties of the ECAP-processed samples, cylindrical samples with a diameter of 6 mm and a gage length of 15 mm were used. Tensile tests were conducted on an Instron tensile testing machine at room temperature and at a temperature of 175 °C with a strain rate of  $10^{-3} \text{ s}^{-1}$ .

Fatigue tests were conducted via the cantilever bending with rotation scheme, at frequency of 50 Hz, under a symmetrical alternating cycle ( $R_\sigma = -1$ ) on the basis of  $N = 10^7$  cycles, using a specially designed machine. On the basis of the test results for a series of samples, fatigue curves were built in the coordinates “maximum stress of a cycle – number of cycles“, and the fatigue endurance limit was determined.

The macrostructure of the fracture surface was investigated using a Lext OLS4000 confocal laser scanning microscope (CLSM) [26], and their microstructure was investigated using a JSM-6390 scanning electron microscope.

## 3. Results and discussion

The structure of the Al-Cu-Mg alloy after solid solution treatment at 530 °C and water quenching was characterized by an average grain size of about 110  $\mu\text{m}$ , as observed by an

optical microscope. The structure contained particles of the  $\text{Al}_9\text{FeNi}$  phase with an average size of 3-6  $\mu\text{m}$ , which had not been dissolved after solid solution treatment.

Several thermal effects related to phase transformations were found in both the quenched and UFG samples heated in a differential scanning calorimeter (Fig. 1). An endothermic peak was revealed in quenched sample at a temperature of 250  $^{\circ}\text{C}$ , turning into an intensive exothermic peak at higher temperatures. In the UFG sample, there was observed a strong reduction in the peak intensity, as well as a displacement of the peak towards lower temperatures, which indicates the occurrence of dynamic aging during SPD processing. According to [27-29], the endothermic peak in coarse-grained Al-Cu-Mg alloys can be caused by dissolution of the Guinier-Preston zones. Study of the structure of the quenched sample subjected to annealing at a higher temperature (260  $^{\circ}\text{C}$ ) has demonstrated that the exothermic peak corresponds to the precipitation of the S phase ( $\text{Al}_2\text{CuMg}$ ), while at grain boundaries there is observed formation of precipitate-free zones of 500 nm in a width (Fig. 2). Note should be made that the appearance of such particles in an Al-Cu-Mg alloy was also observed in [9, 27-29].

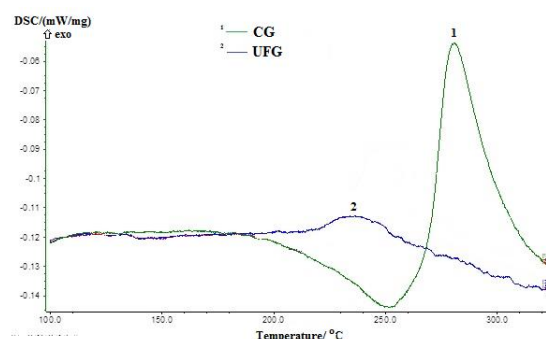


**Fig. 1.** The dependence of heat release on temperature in the Al-Cu-Mg alloy.

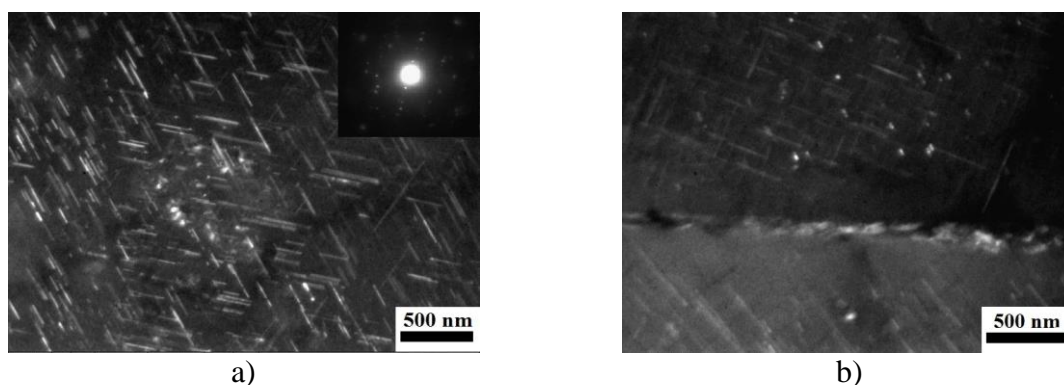


**Fig. 2.** Microstructure of the Al-Cu-Mg alloy after annealing at 260  $^{\circ}\text{C}$ : a) grain body; b) grain boundaries.

Investigation by electron backscatter diffraction has shown that after the standard treatment (T6) the average grain size is of about 200  $\mu\text{m}$  (Fig. 3). The ECAP processing has led to a strong decrease in the size of the structural elements and an increase in the volume fraction of high-angle boundaries.

Study of the microstructure by TEM has shown that in the transverse and longitudinal sections there are observed shear bands with an average width of 200-300 nm (Fig. 4 b,d), and there are also the areas where an ultrafine-grained structure with an average grain size of 250 nm is observed (Fig. 4a,c), thus this structure can be called a bimodal one. Also, there are observed dispersed particles of the phases  $\Theta'$ ,  $\Theta$  and S, having sizes of 10, 40 and 60 nm, respectively (Fig. 5).

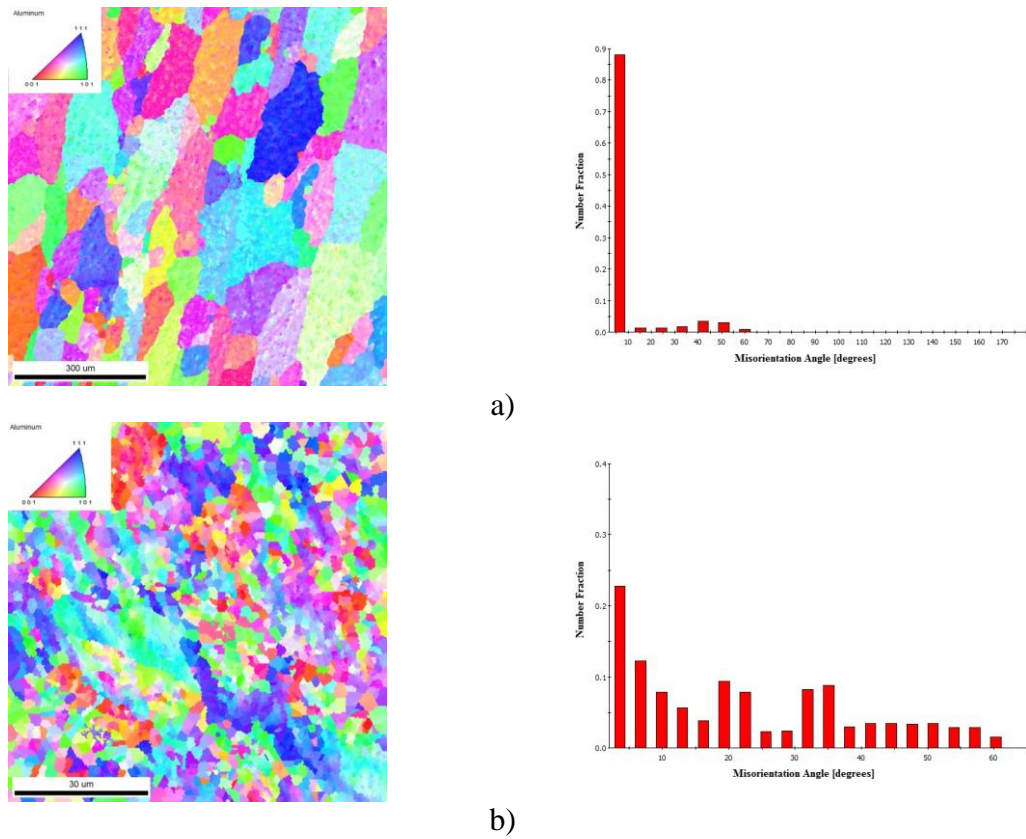


**Fig. 3.** Microstructures and grain boundary misorientation distributions, observed by electron backscatter diffraction after: (a) T6; (b) ECAP processing.

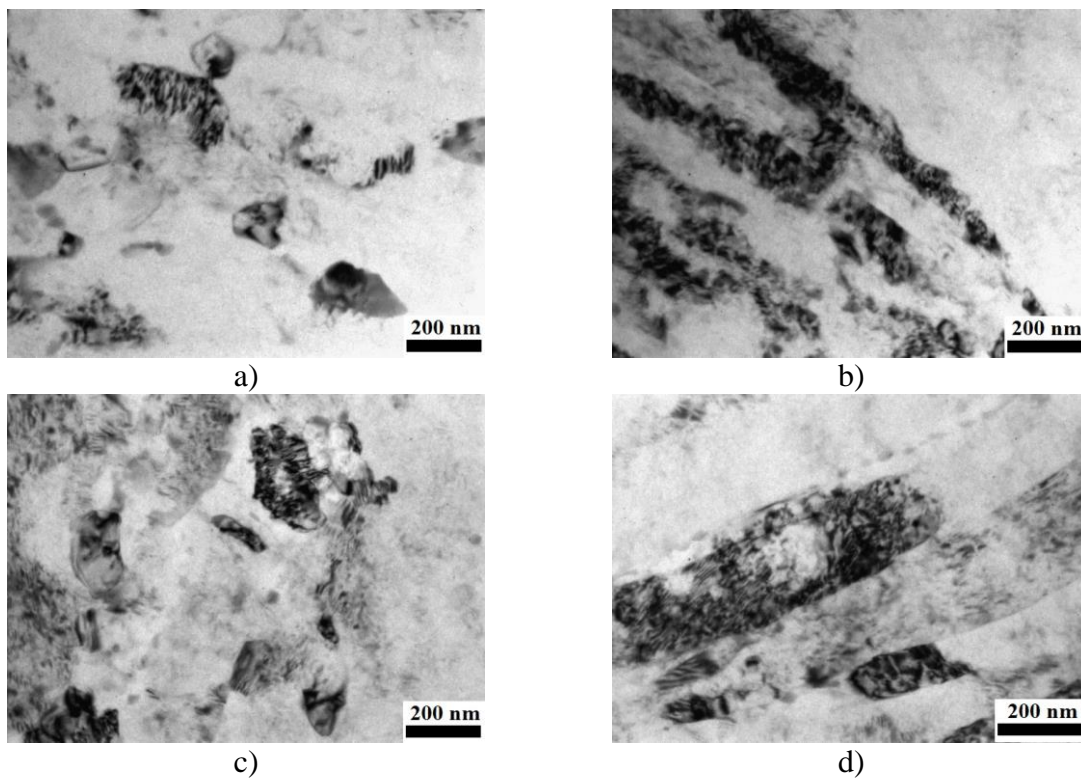


**Fig. 4.** Microstructure of the Al-Cu-Mg alloy after ECAP processing: a,b) longitudinal section; c,d) transverse section.

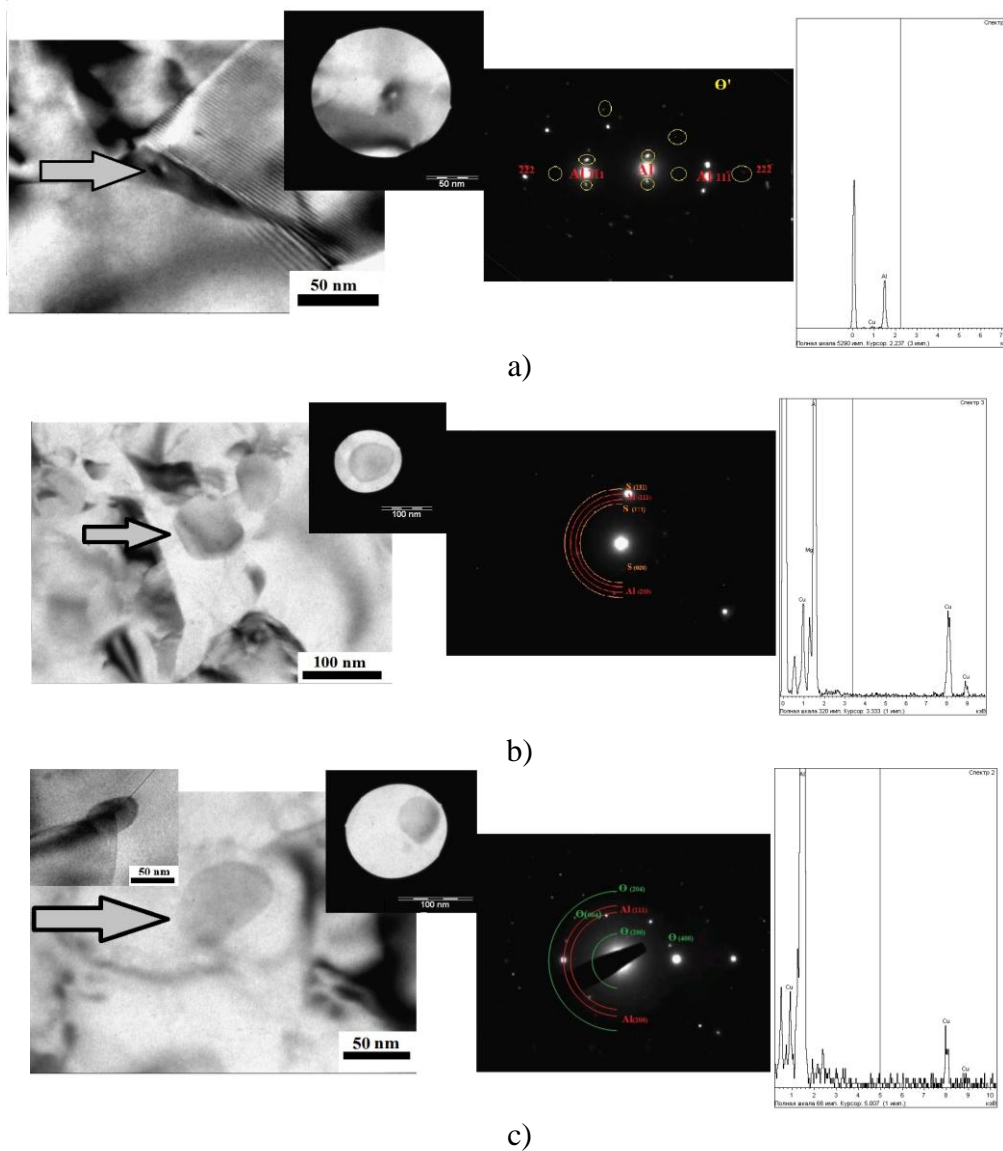


**Fig. 5.** Dispersed particles in the Al-Cu-Mg alloy after ECAP processing: a)  $\Theta'$  ( $\text{Al}_2\text{Cu}$ ); b) S ( $\text{Al}_2\text{CuMg}$ ); c)  $\Theta$  ( $\text{Al}_2\text{Cu}$ ).

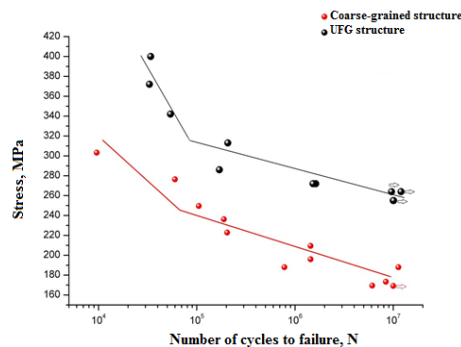
Tests have demonstrated that the microhardness and ultimate tensile strength of the ECAP-processed samples has increased more than 1.5-fold as compared with the samples subjected to the standard T6 treatment (Table 2), while their ductility has decreased in two times. Most probably, the enhanced strength of the UFG samples at room temperature has resulted from a strong grain refinement of the grain structure and precipitation hardening, whereas the reduction in the elongation to failure can be caused by the presence of internal stresses around the particles and in the vicinity of the grain boundaries, affecting on generation and motion of dislocations.

Table 2. Mechanical properties of the Al-Cu-Mg alloy.

Condition	HV	$\sigma_B$ , MPa	$\sigma_{0.2}$ , MPa	$\delta$ , %
T6 (quenching + aging)	$1220 \pm 8$	$370 \pm 7$	$320 \pm 5$	$16 \pm 2$
ECAP	$1980 \pm 20$	$566 \pm 10$	$520 \pm 6$	$8 \pm 1$

Figure 6 shows the results of fatigue tests for Al-Cu-Mg alloy in the condition after the T6 treatment and after ECAP processing. It can be seen that after ECAP processing, the

fatigue endurance limit was 250 MPa, whereas in the condition after the T6 treatment was only 170 MPa. Thus, it can be concluded that ECAP processing enables increasing the fatigue endurance limit of the Al-Cu-Mg alloy approximately 1.5-fold, as compared with the standard T6 treatment. It is evident that the increase in fatigue endurance limit in the ECAP-processed samples was achieved due to a strong grain refinement, as well as the presence of precipitates providing dispersion hardening and shear bands.



**Fig. 6.** The stress amplitude as a function of the number of cycles for the Al-Cu-Mg alloy after T6 treatment (the lower curve) and ECAP processing (the upper curve).

Fracture surface for the CG samples can be subdivided into three distinct zones (Fig. 7a,b). Crack initiation area followed by zone A of stage I crack propagation (zone of stable crack growth), which in turn is followed by zone B of stage II crack propagation (zone of accelerated crack growth) and a final fracture zone C.

The fracture surface, both in the region of low-cycle fatigue and in the region of high-cycle fatigue, have shear steps and ridges in zone A (Fig. 7a,b). The latter is evidently related to the fact that initially several radial fatigue cracks generate at different levels, and joining each other, they form such steps and ridges parallel to the crack growth direction.



**Fig. 7.** Typical fracture surface in the Al-Cu-Mg alloy after T6 treatment: in the low-cycle fatigue region ( $\delta=303,19\text{MPa}$ ,  $N=9,6 \cdot 10^3$ ) (a); high-cycle fatigue region ( $\delta=187,95\text{MPa}$ ,  $N=0,78 \cdot 10^6$ ) (b). The crack initiation zone is located on bottom.

In the region of low-cycle fatigue (Fig. 7a), the final fracture zone C is located in the central part of the fracture surface. The microrelief of the zone of crack propagation consists of separate flat and smooth fragments; secondary cracks are visible (Fig. 8a). Under a large magnification, fatigue viscous striations are observed on the flat fragments (Fig. 8b). The final fracture zone C has a dimple microrelief; particles are visible at the bottom of the dimples (Fig. 8c).

In the fracture surface obtained in the region of high-cycle fatigue (Fig. 7b), two zones can be distinguished: the zone of stable crack growth A and the zone of accelerated crack

growth B [30, 31]. Separate areas of zone A, in spite of the overall macro-irregularity of the surface (Fig. 7b), are relatively smooth, fatigue striations are visible (Fig. 8d). The microrelief of the zone B consists predominantly of flat and relatively smooth fragments (Fig. 8e). The microrelief of the zone C is dimple-type; particles can be seen at the bottom of the dimples (Fig. 8f).

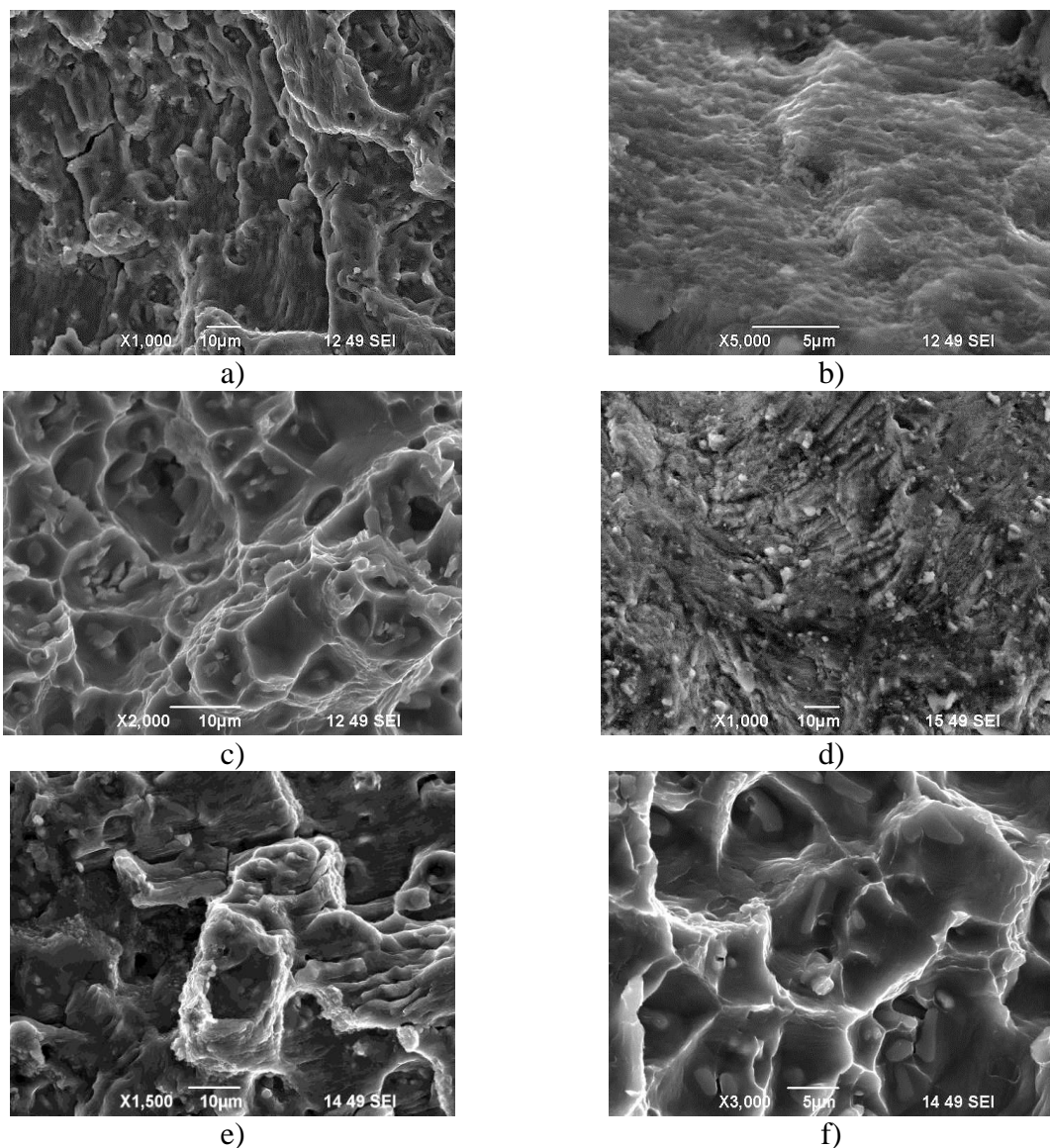


**Fig. 8.** Microrelief of the fracture surface of the Al-Cu-Mg alloy in the T6 condition: the region of low-cycle (a-c) and high-cycle (d-f) fatigue. Zone of crack propagation (a, b); zone A (d); zone B (e); zone C (c, f).

The fracture surface of the Al-Cu-Mg alloy after ECAP processing (Fig. 9a,b) differ from the fractures of this alloy in the T6 condition by a slight roughness and the absence of steps and ridges in the vicinity of the fracture nucleus, which indicates that the fracture starts with the formation of a single microcrack in the fracture nucleus. Here, even in the region of low-cycle fatigue, a small zone A of stable crack growth can be distinguished on the fracture surface (Fig. 9a,c).

The microrelief in the zone A, on the surface of the fractures, obtained both in the region of low-cycle fatigue and in the region of high-cycle fatigue, consists of relatively smooth, viscous fragments (Fig. 10a,d).

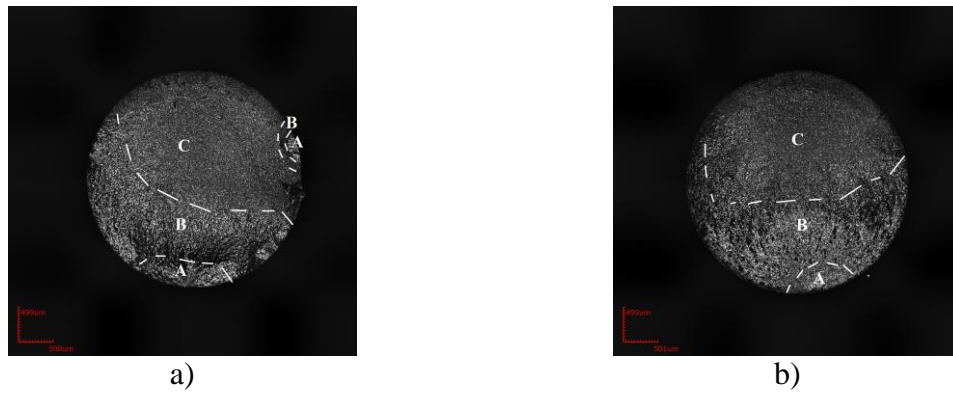


**Fig. 9.** Typical fracture surface in the Al-Cu-Mg alloy after ECAP processing: the region of low-cycle fatigue ( $\delta=372$  MPa,  $N=3,3 \times 10^4$ ) (a); high-cycle fatigue ( $\delta=264$  MPa,  $N=9,6 \times 10^6$ ) (b). The crack initiation zone is located on bottom.

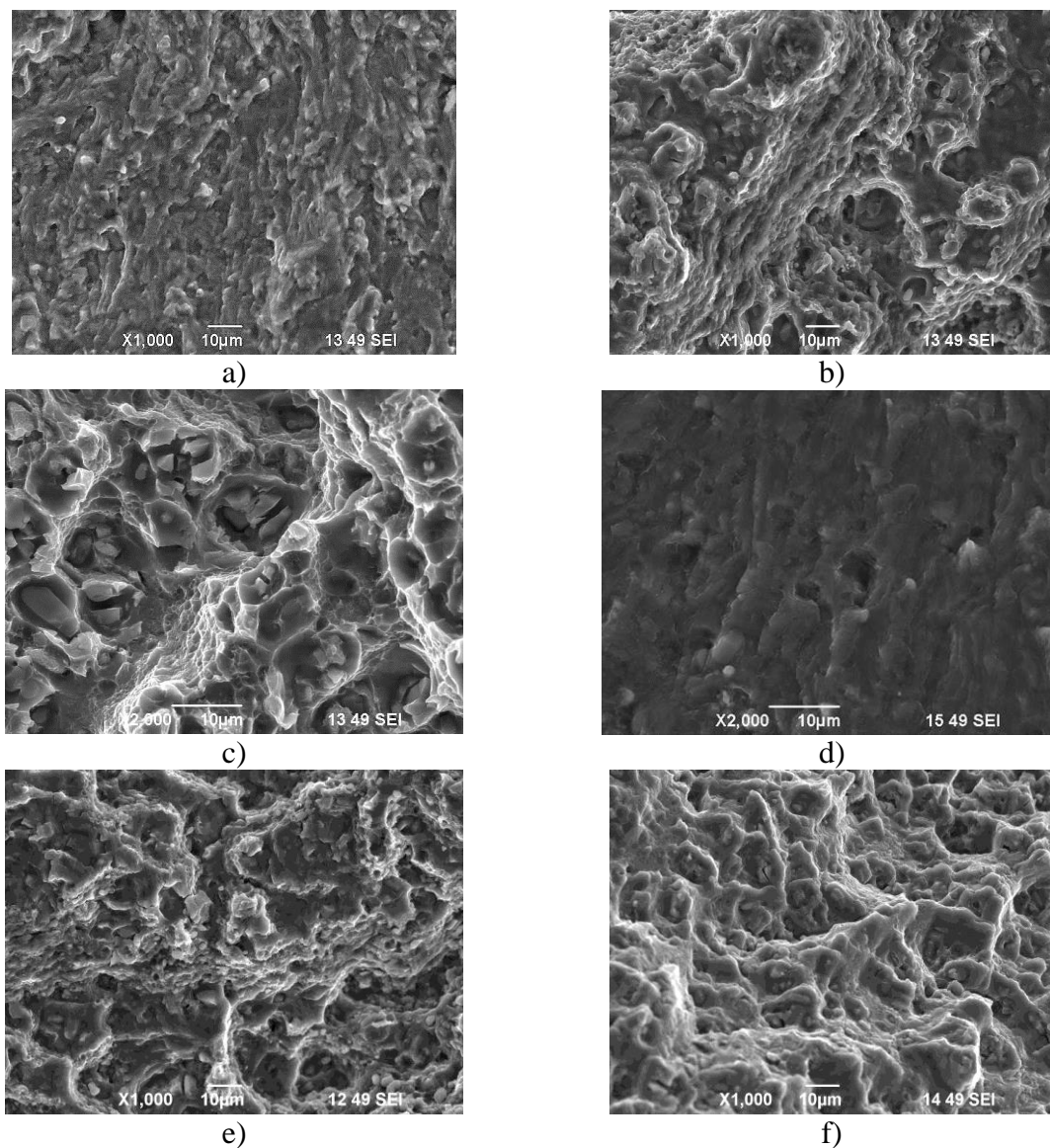


**Fig. 10.** The microrelief of the fracture surface of the Al-Cu-Mg alloy after ECAP processing: in the region of low-cycle (a-c) and high-cycle (d-f) fatigue. Zone A (a, d); zone B (b, e); zone C (c, f).

In the zone of rapid crack propagation B, viscous striations alternate with regions with a dimple microrelief (Fig. 10b,e). The rupture zone has a slight roughness and occupies a large part of the fractures (Fig. 9a,b). The fracture in the rupture zone has occurred viscously with the formation of a dimple microrelief (Fig. 10c,f). In the dimples, particles are observed that have fractured in a brittle manner. There are even more of such particles than in the alloy after the T6 treatment (Fig. 8c,f).

Thus, it has been shown that using ECAP processing it is possible to produce a bimodal structure in an Al alloy of the Al-Cu-Mg system, containing a UFG structure and shear bands. The volume fraction of the UFG structure with an average grain size of 250 nm was 70 %. The shear bands had an average width of 200 nm and occupied 30 % of the studied surface of the ECAP-processed samples. The formation of such a bimodal structure containing dispersed particles enabled increasing the ultimate tensile strength and the fatigue endurance limit by over 50 %. It is evident that the increase in the ultimate tensile strength is conditioned by a strong grain refinement in the UFG component of the ECAP-processed samples and by the presence of dispersed particles. Meanwhile, the considerable increase in the fatigue endurance limit may be related to all the three components (small grain size, dispersed particles and shear bands) which represent additional obstacles on the path of microcrack propagation.

#### 4. Conclusions

From the results obtained one can make the following conclusions.

1. ECAP processing resulted in the formation of a bimodal structure consisting of areas with a UFG structure with an average grain size of 250 nm and shear bands with a width of 200-300 nm. In the structure of the ECAP-processed samples, there was also observed an increased volume fraction of high-angle grain boundaries and the presence of dispersed particles of strengthening phases.
2. The bimodal structure produced by ECAP processing in the Al-Cu-Mg alloy leads to enhancement of ultimate tensile strength and the fatigue endurance limit by more than 50 %, as compared with the samples subjected to the standard T6 treatment.
3. The improvement of the fatigue endurance limit in the ECAP samples of the Al-Cu-Mg alloy can be ascribed to reduced crack propagation rates due to the barrier effect of grain boundaries and dispersed precipitates of strengthening phases.

#### Acknowledgements

*The publication was supported by the Russian Ministry of Education and Science within the basic part of the program for universities and by the Russian Foundation for Basic Research (grant No. 15-38-50445). The work is performed according to the Russian Government Program of Competitive Growth of Kazan Federal University.*

#### References

- [1] R.Z. Valiev, A.P. Zhilyaev, T.G. Langdon, *Bulk Nanostructured Materials: Fundamentals and Applications* (John Wiley & Sons Inc., 2014).
- [2] R.Z. Valiev, R.K. Islamgaliev, I.V. Alexandrov // *Progress in Materials Science* **45** (2000) 103.
- [3] R.Z. Valiev, Y. Estrin, Z. Horita, T. Langdon, M. Zehetbauer, Y. Zhu // *JOM* **58(4)** (2006) 33.
- [4] R.Z. Valiev // *Nature Materials* **3** (2004) 511.
- [5] R.Z. Valiev // *Nanotechnologies in Russia* **1(1-2)** (2006) 208. (In Russian).
- [6] R.Z. Valiev, T.G. Langdon // *Progress in Materials Science* **51** (2006) 881.
- [7] Y. Estrin, A. Vinogradov // *Acta Materialia* **61** (2013) 782.
- [8] E Bobruk, I. Sabirov, V. Kazykhanov, R. Valiev, M. Murashkin // *IOP Conference Series:*

- Materials Science and Engineering* **63** (2014) 012116.
- [9] R.K. Islamgaliev, M.A. Nikitina, A.F. Kamalov // *Materials Science Forum* **667-669** (2011) 331.
- [10] G. Nurislamova, X. Sauvage, M. Murashkin, R. Islamgaliev, R. Valiev // *Philosophical Magazine Letters* **88(6)** (2008) 459.
- [11] O. Kulyasova, R.K. Islamgaliev, B. Mingler, M. Zehetbauer // *Materials Science and Engineering A* **503** (2009) 176.
- [12] I. Sabirov // *Materials Science and Engineering A* **560** (2013) 1.
- [13] M.Yu. Murashkin, I. Sabirov, V.U. Kazykhanov, E.V. Bobruk, A.A. Dubravina, R.Z. Valiev // *Journal of Materials Science* **48(13)** (2013) 4501.
- [14] G. Sha, K. Tugcu, X.Z. Liao, P.W. Trimby, M.Y. Murashkin, R.Z. Valiev, S.P. Ringer // *Acta Materialia* **63** (2014) 169.
- [15] W.J. Kima, C.S. Chung, D.S. Ma, S.I. Hong, H.K. Kim // *Scripta Materialia* **49** (2003) 333.
- [16] W. Huang, Z. Liua, M. Lin, X. Zhou, L. Zhao, A Ning, S. Zeng // *Materials Science and Engineering A* **546** (2012) 26.
- [17] E.V. Bobruk, M.Yu. Murashkin, V.U. Kazykhanov, R.Z. Valiev // *Reviews on Advanced Materials Science* **31** (2012) 14.
- [18] I.G. Brodova, I.G. Shirinkina, A.N. Petrova, O.V. Antonova, V.P. Pilyugin // *The Physics of Metals and Metallography* **111(6)** (2011) 630.
- [19] J. Gubicza, I. Schiller, N.Q. Chinh, J. Illy, Z. Horita, T.G. Langdon // *Materials Science and Engineering A* **460-461** (2007) 77.
- [20] Y. Estrin, A. Vinogradov // *International Journal of Fatigue* **32** (2010) 898.
- [21] V. Patlan, A. Vinogradov, K. Higashi, K. Kitagawa // *Materials Science and Engineering A* **300** (2001) 171.
- [22] A. Washikita, K. Kitagawa, V.I. Kopylov, A. Vinogradov, In: *Ultrafine grain metals II, TMS*, eds. Y.T. Zhu, T.G. Langdon, R.S. Mishra, S.L. Semiatin, M.J. Saran, T.C. Lou (TMS, 2002), p. 341.
- [23] J. May, M. Dinkel, D. Amberger, H.W. Höppel, M. Göken // *Metallurgical and Materials Transactions A* **38** (2007) 1941.
- [24] H.W. Höppel, M. Brunnbauer, H. Mughrabi, R.Z. Valiev, A.P. Zhilyaev, In: *Proceedings of Werkstoffwoche* (2000; 2001).
- [25] Y. Wang, M. Chen, F. Zhou, E. Ma // *Nature* **419** (2002) 912.
- [26] G.V. Klevtsov, E.D. Merson // *Fundamental Research* **11(5)** (2012) 1185. (In Russian).
- [27] S.C. Wang, M.J. Starink // *International Materials Reviews* **50** (2005) 193.
- [28] G.W. Smith, W.J. Baxter, R.K. Mishra // *Journal of Materials Science* **35** (2000) 3871.
- [29] G.W. Smith. // *Thermochimica Acta* **317** (1998) 7-23
- [30] S. Kocanda, *Fatigue Cracking of Metals*, ed. by S.Ya. Yarema (Metallurgiya, Moscow, 1990). (In Russian. Translated from Polish).
- [31] G.V. Klevtsov, L.R. Botvina, N.A. Klevtsova, L.V. Limar, *Fracture Diagnostics in Metallic Materials and Structures* (MISiS, Moscow, 2007). (In Russian).